JOURNAL OF MATERIALS SCIENCE 29 (1994) 2025–2039

Heat transfer aspects of splat-quench solidification: modelling and experiment

T. BENNETT, D. POULIKAKOS
Mechanical Engineering Department, University of Illinois at Chicago, PO Box 4348, Chicago, IL 60680, USA

In this paper a combined theoretical and experimental study is reported on the process of solidification of a liquid metal droplet by impaction on a cold substrate (splat-quenching). The study is focused on the heat transfer aspects of this process and on the identification of parameters affecting the heat transfer mechanism. To this end, the effect of the droplet impact velocity and temperature, the effect of the substrate material and its initial temperature, and the effect of the thermal contact resistance between the splat and the substrate are investigated. A two-dimensional conduction model accounting for the freezing process in the splat and for the solidification kinetics has predicted reasonably well the trends observed in the experimental part of the study.

Nomenclature

c	Specific heat
D	Droplet diameter
g	Gravitational acceleration
h_a	Heat transfer coefficient between splat and ambient
h_c	Heat transfer coefficient for splat–substrate interface
H	Thickness of splat
k	Thermal conductivity
K_f	Freezing kinetics coefficient
L	Free-fall distance
L_f	Latent heat of freezing
Nu_D	Nusselt number (hD/k)
Pr	Prandtl number (ν/α)
r	Radial distance
R	Radius of splat
Re	Reynolds number (uD/ν)
t	Time
t_c	Free-fall time
T	Temperature
T_f	Freezing temperature of splat
T_i	Freezing interface temperature
T_0	Substrate temperature
T_∞	Ambient temperature
ΔT_c	Temperature drop across the splat–substrate interface
u	Impact velocity of droplet
V	Freezing interface velocity
z	Axial distance
α	Thermal diffusivity
ν	Kinematic viscosity
θ	Instantaneous temperature difference between falling droplet and ambient
θ_a	Initial temperature difference between falling droplet and ambient

Subscripts

l	Liquid phase
s	Solid phase

1. Introduction

Splat-quenched solidification is a rapid solidification process which, as its name indicates, involves the impingement, spreading and ensuing solidification of a liquid metal droplet on a solid substrate. This process is one member of a family of spray deposition regimes [1–3]. These regimes are distinguished by the conditions existing on the deposition surface as well as the state of the impinging spray itself. In the case of splat-quenched solidification, consecutive generations of entirely liquid molten droplets impact upon a completely solidified surface. This situation occurs when the mechanism of heat transfer (principally conduction) away from the deposition layer is capable of removing heat much faster than it is deposited in the form of molten material. When the sprayed material is splat-quenched on to the deposition surface, fusion between consecutive generations of deposited material tends to be poor, because there is usually insufficient heat in the impinging spray to liquefy prior deposits. The deposition is marked by microstructure characterizing very rapid solidification. The continuity of the deposition layer is interrupted by discrete boundaries between individually deposited material and small amounts of oxides (if the deposition is not performed in an inert environment). Pores may also reside at these boundaries.

Manufacturing industry has taken an interest in spray deposition technology because of its near-net shaping capability and rapid preform production, as

0022–2461 © 1994 Chapman & Hall

well as improved material properties [3–5]. This route of manufacturing is particularly attractive for working with alloys where problems arising from segregation, brittle phases and large grain size make conventional methods inappropriate [5].

Focusing on the process of splat-quenching solidification, one of the most frequently utilized rapid solidification processes, it is easy to discover that a significant amount of work has been performed to study the basic mechanisms of this process, especially from the materials science standpoint. Jones [1] and Anantharaman and Suryanarayana [6] have summarized the first decade of developments resulting from the application of the splat-quenching technique.

Predecki *et al.* [7] performed a study to determine solidification rates, heat-transfer coefficients and cooling rates in splats. They studied not individual droplets but a spray produced from a few tenths of a gram of molten metal with the "gun" technique. Predecki *et al.* demonstrated clearly a couple of defining characteristics of the splat-quenching process, the first being that cooling rates imposed on the splat are extremely high, and the second, that the freeze propagates very rapidly through the melt.

Brower *et al.* [8] performed a comparative study of the relative cooling rate and its effect on microstructure, for cooling imposed by gas quenching, liquid quenching, chill casting and splat quenching. Scott [9] made comparative measurements of the average and maximum cooling rates exhibited by aluminium copper alloy splats quenched on copper and glass (soda glass) substrates. He found the surprising result that the cooling rate of a splat on a glass substrate was higher than the cooling rate of the same splat on a copper substrate. He explained his results by suggesting that because of glass melting, the thermal contact between the splat and the substrate was much better for the glass substrate than the copper substrate.

Numerical investigations of the heat transfer and solidification aspects of splat-quenched solidification generally fall within two categories: modelling of the one-dimensional rapid solidification of a melt [10–14], and comprehensive modeling of an entire spray deposition system [3, 15, 16]. The first area is principally interested in the kinetics of the freezing process and its bearing on the microstructure of the resulting solid. The second area is concerned more with process parameters of commercially available systems, and their impact on the performance of those systems. In the following paragraphs we will briefly discuss representative studies of the first area since they are directly related to the present work. Wang and Matthys [10, 11] have investigated the interface velocity as a function of propagation distance, with and without undercooling of the melt, using a one-dimensional conduction model. With undercooling, the velocity of the interface is seen to decrease rapidly as the freeze propagates. Without undercooling of the melt, the velocity of the interface is heat-transfer-limited, realizing a less drastic change in interface velocity as the front propagates forward. The quality of thermal contact between splat and substrate is influential in sustaining the interface velocity in an undercooled melt and critical if there is no undercooling.

Relevant to the splat quenching process was the work of Shingu and Ozaki [12] who investigated numerically rapid solidification occurring by conduction cooling. Rosnar and Epstein [13] studied theoretically the simultaneous kinetic and heat transfer limitations in the crystallization of highly undercooled melts. Evans and Greer [14] developed a one-dimensional numerical solution to the rapid solidification of an alloy melt in order to investigate solute trapping. Their model employed two equations relating the interface velocity and solid composition to the temperature and liquid composition at the freezing interface.

The work presented in this paper aims at improving our understanding of the heat transfer process during the splat-cooling and solidification of a liquid metal droplet impacting upon a cold substrate. To this end, a two-dimensional conduction model accounting for solidification and based on crystallization kinetics theory is constructed and solved. Utilizing this model, the process parameters influencing the solidification are identified. The accuracy of the model is tested with a simple experiment that yields results on the temperature and the heat transfer rates at the splat–substrate interface. Electron microscopy is also utilized selectively to determine the effect of the substrate material on the structure of the solidified splat.

2. Experimental procedure

The goal of the experimental study is twofold: first, to establish the effect of the substrate material, substrate temperature and droplet impact velocity on the temperature and the heat transfer rate at the splat–substrate interface, as well as on the microstructure of solidified splats, and second, to test the validity of the numerical model.

The production of uniformly sized molten droplets was achieved with a resistively heated ceramic "dropper tube". The dropper tube, pictured in Fig. 1, operates by gravity feed, such that the size of the droplet is governed by the surface tension and weight of the molten material, and by the exit orifice diameter of the dropper tube. With an orifice diameter of 790 μm the dropper tube produced 3.0 mm diameter droplets with a standard deviation of 10%. The superheat established at the formation of the droplet was in the range 130 to 190 °C above freezing temperature and was controlled by the amperage delivered to the resistive heating coil. The temperature of the superheated droplet during formation was measured by a K-type thermocouple implanted in the tip of the dropper tube.

The droplet impact velocity was attained by allowing the droplet to free-fall a determined distance between the dropper tube tip and the substrate surface. The amount of cooling of the droplet incurred during free fall was estimated by a Nusselt number correlation for a freely falling sphere [17]. The details of this calculation are contained in the Appendix. The temperature of the splat–substrate interface was measured with a foil, fast response, K-type thermocouple moun-

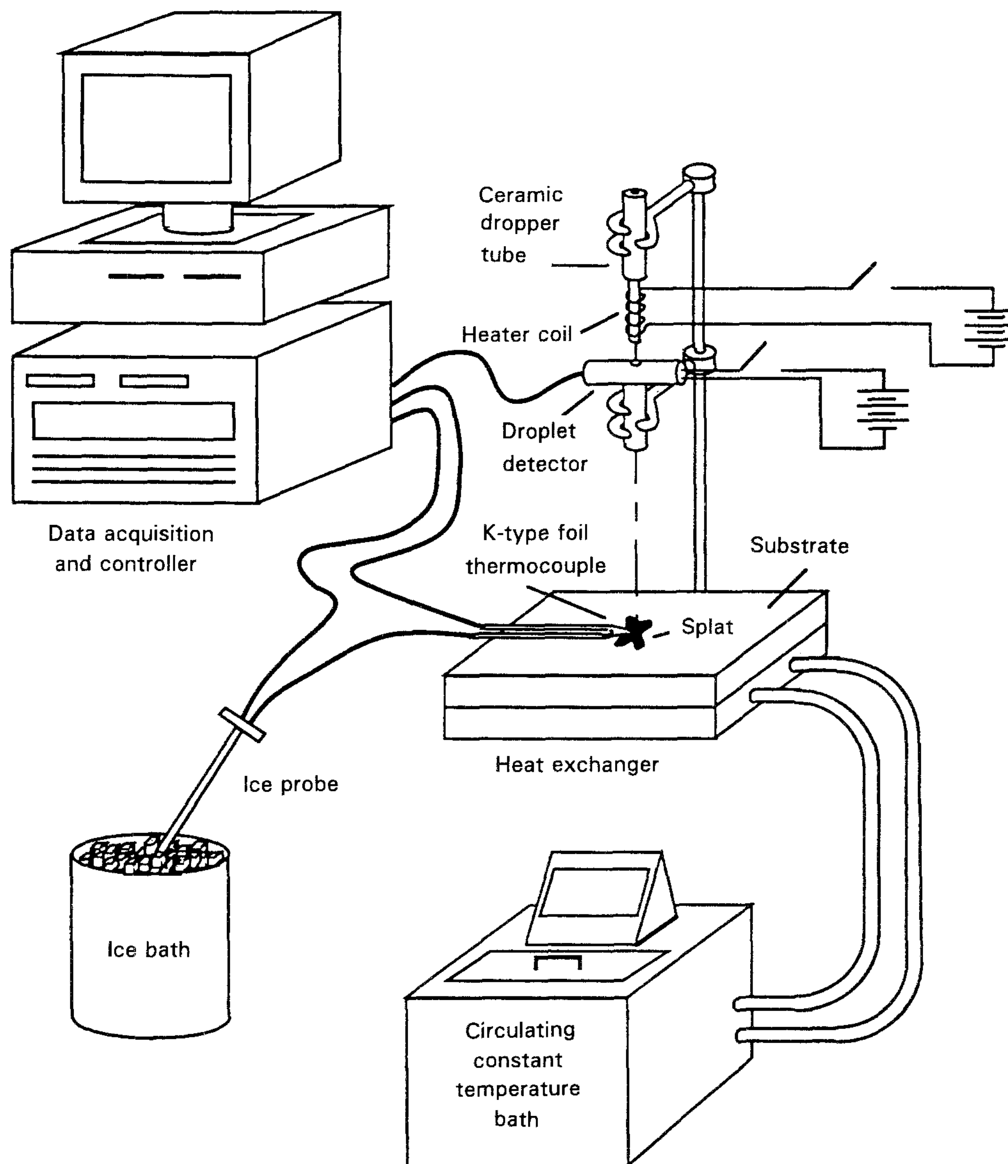

Figure 1 Schematic diagram of experimental apparatus.

ted on the substrate surface with a thermally conductive epoxy cement (Omega Inc, Stamford, CT, USA). The foil thickness was 12.7 μm. The voltage output of the thermocouple was collected by an HP 3852 data acquisition system connected to an HP Vertra computer (Fig. 1). The droplet temperature at impact, estimated as shown in the Appendix, was utilized in the theoretical model (Section 3) as the temperature of the droplet at the time of initial contact with the substrate, in order to facilitate the comparisons between the theory and experiment. Note that this estimate is deemed to be more accurate than the thermocouple output at impact which is hampered by the inertia effect of the thermocouple.

Because of the extremely high sampling rate used, and the limited storage space of the data acquisition system, the period of time over which the thermocouple temperature could be monitored was limited to less than 3 s. Consequently, it was necessary to devise a droplet detection system to automatically initiate the data acquisition just prior to quenching of the droplet. A droplet detector was fashioned from a photocell and light source, such that the light beam directed on the photocell would be interrupted by the falling droplet. The output from the photocell was monitored by one channel of the data acquisition system so that when the falling droplet was detected, the data acquisition system would switch channels and begin measuring the voltage output of the thermocouple affixed to the substrate surface.

The droplet impact velocity, controlled by the free-fall distance, was varied between 1.7 and 2.4 $m\,s^{-1}$ (15 to 30 cm free-fall distance). These velocities were estimated by assuming that the droplet is falling freely in the gravitational field (see Appendix). The lowest impact velocity was limited by the closest distance to the substrate surface from which the droplet could be released and still have sufficient time for the data acquisition system to detect the droplet and initiate data collection. The highest impact velocity was limited by the cohesion characteristics of the droplet on impact. At higher impact velocities the droplet tended to break apart, leaving the thermocouple exposed.

The substrate materials were selected on the basis of their thermal conductivities. Copper, aluminum and Pyrex were chosen as having high, intermediate and

low thermal conductivity, respectively. Teflon was also considered, having an extremely low thermal conductivity, but was abandoned because of the inability of the thermocouple epoxy cement to adhere to its surface. The temperature of the substrate was controlled with a heat exchanger attached to its bottom (Fig. 1). An ethylene glycol and water mixture was circulated through the heat exchanger. The temperature of this mixture was controlled with a Birkman RC20 constant temperature bath circulator that had a temperature range of − 30 to 150 °C.

The droplet material selected was lead, because of its low melting point and easy handling characteristics. All the droplet material properties utilized in this study are those of lead. The high density of lead also facilitated the production of "small" droplets without using an excessively small orifice on the dropper tube. This is an important consideration because, although small droplets of any size could theoretically be produced if the orifice was sufficiently small, in practice this was not the case; if the orifice becomes too small, it is difficult to gravity-feed the droplet through the opening. Furthermore, the smaller orifice sizes are especially prone to choking, caused by build-up of residual oxides, with continued use. The use of lead, having high specific weight, overcomes the capillary forces that retain the droplet with a relatively small build-up of volume, yielding a small droplet diameter.

The procedure adopted in the collection of data was straightforward. Initially, the dropper tube tip temperature and the substrate temperature are brought to their desired values by adjusting the amperage applied to the heater coil on the dropper tube and by regulating the temperature of the circulating bath, respectively. Both of these temperatures can be monitored through the data acquisition system. The free-fall distance to the substrate surface is adjusted by sliding the dropper tube bracket up or down its mounting post. After these initial parameters are established, the data collection program is initiated, and the acquisition system waits for a droplet to be detected.

A molten droplet is produced by feeding, one at a time, slugs of the metal wire into the dropper tube. The wire melts in the body of the dropper tube, and is forced through the tip orifice by its own body weight. A droplet forms at the tip of the dropper tube until it becomes sufficient in weight to detach itself. The droplet detector senses the falling droplet and initiates the collection of data, which are then automatically displayed as a temperature versus time curve on the screen of the controller. The weight of the splat is measured directly using a precision scale.

The molten droplets were splat-quenched and their temperature traces recorded every 10 °C (approximately) as the substrate was heated from 10 to 100 °C. For each substrate material, the range of temperatures was spanned twice, once for a free-fall distance of 15 cm, and a second time for a free-fall distance of 30 cm. Additionally, for the aluminium substrate at room temperature, the free-fall distance was varied from 15 to 30 cm increments, to further investigate the effect of impact velocity.

3. The theoretical heat transfer model

The theoretical part of this study models the heat-conduction-induced solidification in the metal splat. Invoking a simple order-of-magnitude analysis, it can be shown that the liquid metal droplet, after impact upon the substrate, spreads first and solidifies subsequently. This result was also observed in the experiments of the present study. Therefore, since we aim to propose a relatively simple and easy-to-use model, the effect of convection due to the spreading process on the freezing of the splat is neglected.

The splat is modelled as a thin liquid metal disc initially at uniform temperature T_∞, which is suddenly brought into contact with a large (by comparison) substrate of initial temperature, T_0, considerably lower than the freezing temperature of the splat material, T_f. Heat is conducted away from the splat into the substrate. Solidification ensues and progresses until the entire splat is solidified. The heat-conduction cooling of the splat continues after solidification is completed, until the splat temperature reaches the substrate temperature.

The heat conduction process is modelled as two-dimensional both in the splat and the substrate. To this end, the range of validity of previous one-dimensional models will be explored. The conduction equation describing the transport of heat in the splat with respect to the cylindrical coordinate system (r, z) of Fig. 2 is

$$(\rho c)_j \frac{\partial T_j}{\partial t} = k_j \left[\frac{\partial^2 T_j}{\partial r^2} + \frac{1}{r}\left(\frac{\partial T_j}{\partial r}\right) + \frac{\partial^2 T_j}{\partial z^2} \right] \quad j = \mathrm{l, s} \tag{1}$$

where the subscript j takes on the values l or s when Equation 1 is applied to the liquid or to the solid portion of the solidifying splat, respectively. The temperature is denoted by T_j, the time by t, and the thermal conductivity, density and specific heat of the splat by k_j, ρ_j and c_j, respectively. Equation 1 reflects the independence of the heat transport of the angular position from symmetry considerations.

The heat conduction equation in the substrate is

$$\rho c \frac{\partial T}{\partial t} = k \left[\frac{\partial^2 T}{\partial r^2} + \frac{1}{r}\left(\frac{\partial T}{\partial r}\right) + \frac{\partial^2 T}{\partial z^2} \right] \tag{2}$$

in which the notation is analogous to that defined earlier after Equation 1.

To complete the model formulation, the relevant initial, boundary and matching conditions need to be discussed. The initial conditions of the problem are that both the substrate and the splat were isothermal prior to making contact with one another: at $t = 0$

$$T_l = T_\infty \tag{3}$$

$$T = T_0 \tag{4}$$

The boundary conditions at the top and at the lateral surface of the splat are, for $z = H$,

$$k_j \frac{\partial T_j}{\partial z} = h_a (T_j - T_a) \quad j = \mathrm{s, l} \tag{5}$$

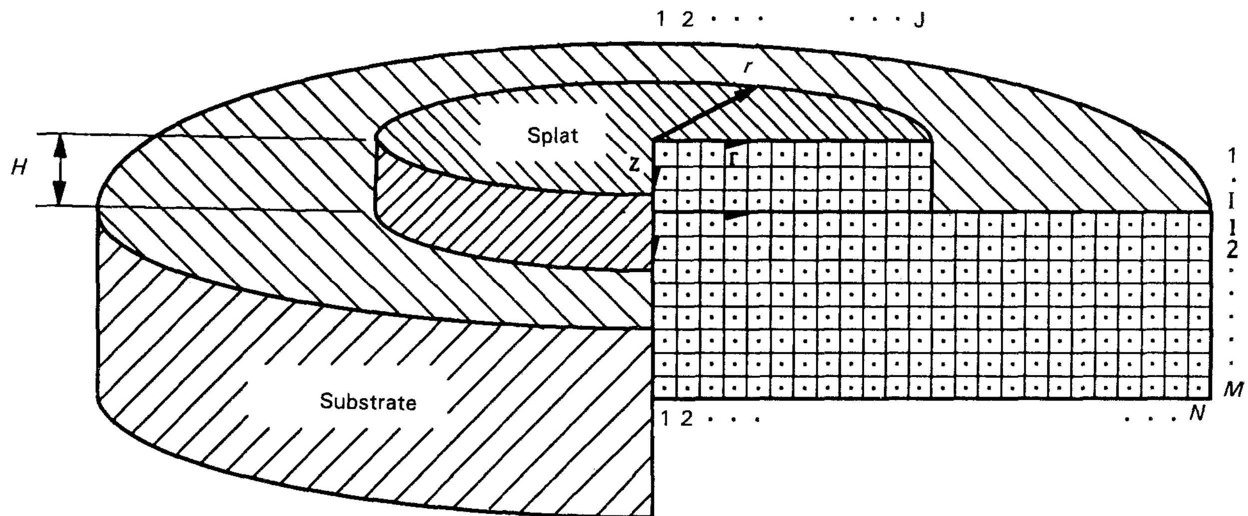

Figure 2 Nodal grid for splat–substrate system.

and for $r = R$

$$-k_j \frac{\partial T_j}{\partial r} = h_a(T_j - T_a) \qquad j = s, l \tag{6}$$

where h_a is the heat transfer coefficient between the splat surface and the ambient, and T_a is the ambient temperature. These boundary conditions account for the convective removal of heat from the splat surface. A similar boundary condition to Equation 5 accounts for convection of heat from the top surface of the substrate.

Since freezing takes place in the splat, the solid and the liquid regions are separated by a freezing interface. The matching conditions for the temperature field at this interface are, for $z = z_i$,

$$T_s = T_l \tag{7}$$

$$-\rho_s L_f V = k_l \frac{\partial T_l}{\partial z} - k_s \frac{\partial T_s}{\partial z} \tag{8}$$

The subscript i denotes the position of the freezing interface. Conditions 7 and 8 stand for the temperature continuity and for heat flux discontinuity because of the heat released upon solidification. The negative sign in the left-hand side of Equation 8 reflects the fact that the freezing interface velocity is pointing to the negative z-direction. Note that in writing Equation 8, the radial conduction was neglected for simplicity. This approximation is certainly appropriate since the splat thickness is two orders of magnitude smaller than the splat diameter.

The matching conditions at the splat–substrate interface are as follows:

$$z = H \quad -k_j \frac{\partial T_j}{\partial z} = h_c \Delta T_c \qquad j = s, l \tag{9}$$

This condition can alternatively be written for the substrate side of the interface

$$z = H \quad -k \frac{\partial T}{\partial z} = h_c \Delta T_c \tag{10}$$

The above matching conditions account for the presence of a contact thermal resistance at the splat–substrate interface. To this end, Condition 9 states the fact that the heat flux leaving the splat at the interface equals the product of a heat transfer (resistance) coefficient descriptive of the imperfect thermal contact at the interface, multiplied by the temperature jump across the interface (ΔT_c) defined as the difference between the interface temperatures at the splat and the substrate sides. Condition 10 is analogous to Condition 9 written for the substrate side of the interface.

The temperature of the substrate far away from the interface is not affected by the presence of the splat:

$$z \rightarrow \infty \qquad T \rightarrow T_0 \tag{11}$$

The last issue to be discussed before completing the description of the heat conduction model is the undercooling present in the splat at the initiation and subsequent development of the solidification process [10, 12]. In the classical treatment of a freezing front, the front is defined by the freezing temperature of the material and its propagation velocity is limited by the rate at which heat can be conducted away from this front into the liquid and solid regions (Equation 8). However, this treatment does not account for the presence of undercooling in the melt prior to the initiation of solidification. Such undercooling is a common occurrence in the splat-quenching process and other rapid solidification processes, and results in the freezing front being at a temperature below the equilibrium freezing temperature. To account for this fact, a freezing kinetics relationship between the amount of undercooling and the velocity of propagation of the freezing interface is needed. A popular relationship of this kind postulates a linear dependence of the freezing front propagation velocity on the amount of undercooling [10, 11]:

$$V = K_f(T_f - T_i) \tag{12}$$

where K_f is a freezing kinetics coefficient, T_f the equilibrium freezing temperature of the solid–liquid interface and T_i the actual temperature of this interface.

If undercooling exists and T_i is below T_f Equation 12 will result in a rate of latent heat release in excess of that which can be conducted away from the interface. In this limit, the propagation of the solidification front is said to be controlled by the freezing kinetics. The rapid propagation of the freezing interface will cause its heating and subsequent retardation of its propagation. As the freezing interface temperature approaches the equilibrium freezing temperature, the solidification becomes heat-transfer-limited.

At this point, the mathematical formulation of the heat conduction model is complete. The methodology of the numerical solution is discussed next. The numerical solution of the model described earlier was obtained with the finite difference discretization method. To this end, the splat was overlayed with a network of I grid points in the axial direction and J grid points in the radial direction. An analogous $(M \times N)$ grid network was defined for the substrate. The grid spacing in the radial direction (Δr) was not constant and it was larger than that of the axial direction (Δz). The finite differences allowed for the utilization of different grid spacings in the axial and radial directions in the substrate and in the splat.

The mathematical model consisting of Equations 1–12 was discretized by invoking the control volume method [18]. After discretization, the resulting system of algebraic equations was solved with the ADI method [18]. No details of the discretization process are included here for brevity and because they can be found explained at great length elsewhere [19]. Regarding the fineness of the time and space grid size, grid independence was established for all results presented in this paper [19]. Early in the freezing process, the duration of the time step was shortened to 10^{-9} s. Subsequently, the time step was permitted to increase as the rate of changing thermal conditions deemed permissible. Time steps were controlled dynamically for optimal performance and ranged between 10^{-9} and 10^{-6} s throughout the course of the cooling process. Short time steps were required during the earliest period subsequent to initial thermal contact and during freezing. Longer time steps were used when changes in thermal conditions were gradual. Typically 100 nodes were used in the splat and 250 nodes in the substrate. The axial spacing between the nodes ranged between 1 and 10 μm in the splat and 10 to 1000 μm in the substrate. Radial spacing ranged from 50 to 1000 μm both in the splat and the substrate.

The numerical computation marched forward in time as follows. First, the current thermal and phase conditions of the splat were checked. Freezing of the splat was initiated when any one of the bottom surface nodes of the splat reached a temperature below the prescribed degree of undercooling. At this point any or all of the splat nodes, below the melting temperature, may commence freezing, as governed by the freezing kinetics model. For all computations presented in this section, an initial undercooling of 40 °C was prescribed. This degree of undercooling was estimated on the basis of the experimental observations of the following section. If freezing was present in the current time step, the freezing interface was moved forward a distance equal to the product of the interface velocity and one full time step. The velocity of the freezing interface was determined from Equation 12, using the temperature of the freezing interface during the previous time step.

Utilizing the updated physical conditions, the solution was advanced by one time step with the ADI procedure. At the end of one time step, the rate of change of the temperature field was checked. If the change of the temperature field between the current time step and the previous time step was very small, the size of the future time step was increased accordingly to speed up the calculation and then the cycle was repeated.

The numerical code typically required about 60 CPU s to solve for the first 0.5 s of the quenching process on the IBM RS6000. However, the exact computational time was dependent on the nodal system used; the maximum allowable time step is limited by the smallest nodal spacing used. Although the time step was dynamically controlled, the nodal grid was fixed for the duration of the computation, imposing an upper bound on the time step size (usually about 1 μs).

4. Results and discussion

In the discussion of results, key experimental findings will be presented first. Next, comparisons between theoretical and experimental results will put into perspective the validity of the numerical model. Finally, additional numerical results will provide information for aspects of the problem not available experimentally.

Although quite often initial cooling information was suppressed by sluggish thermocouple response, ample experimental data were taken to establish thermal conditions at and just prior to freezing. Fig. 3a and b present splat–substrate interface temperature and cooling rate traces, for splats quenched from approximately the same initial temperature (480 °C) on heated (90 °C) copper and Pyrex substrates. The spread factor appearing in the legend of these and subsequent figures is defined as the ratio of the final splat diameter to the initial droplet diameter.

Figure 3a shows the temperature versus time traces in which the first 100 ms of the quenching process have been detailed. The discontinuity in the slope of the curve at about 10 ms into the quenching process represents the release of latent heat during solidification of the splats. It is apparent that freezing is initiated well below the melting temperature of lead (328 °C). This confirms the fact that undercooled conditions are prevalent during splat-quenched solidification, an important attribute accounting for many of the novel microstructural features yielded by this process.

Additional information is shown in Fig. 3b, which presents the cooling rates of the aforementioned two splats at the substrate surface as a function of time. Presented in this form, we are better able to discern the moments in which freezing of the melt begins and ends. In this particular case, both of the splats quenched on the copper and Pyrex substrates initially

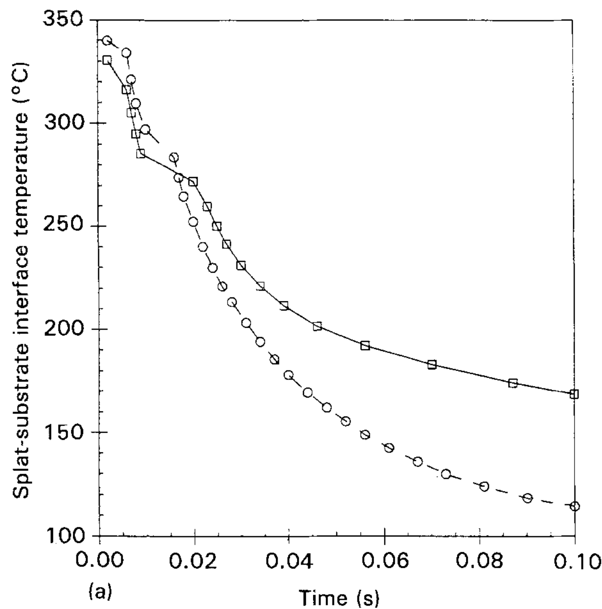

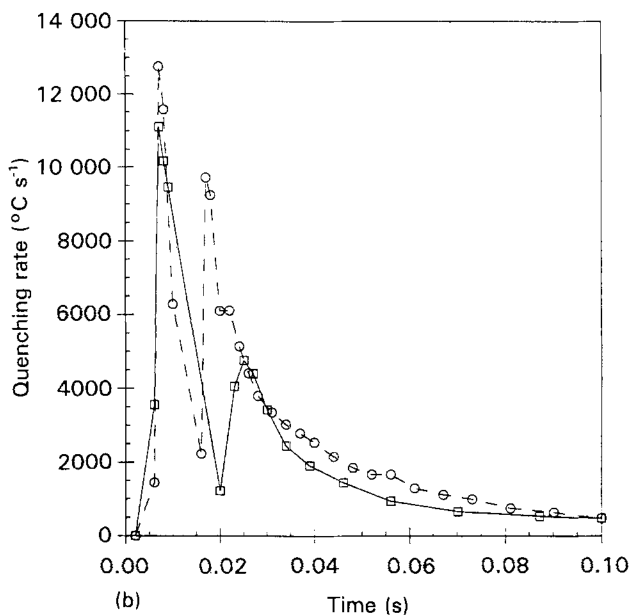

Figure 3 Thermal history of splat subsequent to impact with copper and pyrex substrates: (a) splat–substrate interface temperature versus time, (b) splat-quenching rate versus time. Data represented by the following conditions for (○) Copper and (□) Pyrex, respectively: initial droplet temperature 480/480 °C, initial substrate temperature 90/90 °C, droplet diameter 3.0/3.0 mm, free-fall distance 30/30 cm, spread factor 4.2/4.3.

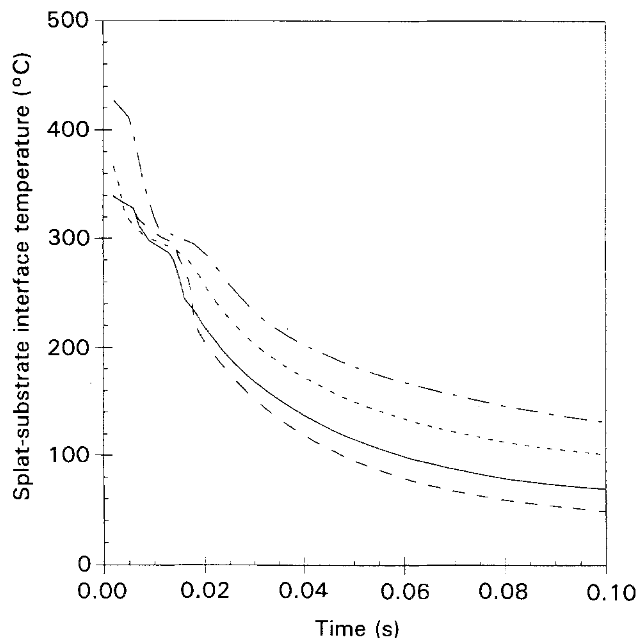

Figure 4 Effect of substrate temperature on the thermal history of splat. Data represented by the following conditions for T_0 = (– –) 25 °C, (——) 50 °C, (---) 71 °C and (– - –) 100 °C, respectively: initial droplet temperature 470/475/469/470 °C, droplet diameter 3.0/3.0/3.1/3.0 mm, free-fall distance 30/30/30/30 cm, spread factor 4.1/4.1/4.3/4.2.

began to freeze 7 ms after making thermal contact with the substrate. The splat quenched on the Pyrex substrate completed freezing 18 ms later, while the splat quenched on the copper substrate completed freezing in only 10 ms. The substantial difference in duration of freezing reflects the relative ability of the two substrate materials to sustain high cooling rates.

The next issue to be addressed is the effect of substrate temperature on the splat-quenched solidification process. One expects that increasing the substrate temperature will adversely affect its ability to impose high cooling rates on the splat. Heat transfer away from the splat is governed by the thermal gradients below the splat, which are established by the initial temperature difference between the splat and substrate materials.

Figure 4 demonstrates the effect of the initial substrate temperature on the thermal history of splats quenched on copper. The most distinctive effect of the substrate temperature is on the asymptotic approach of the splat temperature toward that of the substrate. However, the curves corresponding to different initial substrate temperatures are qualitatively similar.

There are several motivations for a close inspection of the splat after solidification. The most obvious one, and the most frequently investigated, is the effect of the rapid solidification on the microstructure of the splat. Motivation is also borne in determining large-scale geometric characteristics of the solidified splat, which will be beneficial in evaluating some of the assumptions made in the numerical heat transfer modelling of the splat. Additionally, inspection of the contact surface may allow for qualitative assessments to be made concerning the quality of thermal contact between the splat and the substrate. Because of the aforementioned reasons typical splats were examined with electron microscopy. The results are shown in the photographs of Figs 5–7.

The photographs in Figs 5 and 6 correspond to the top surface of splats solidified on different substrates and feature dramatically different surface structures. One discernible feature on the top surfaces of splats quenched on the copper, aluminium and Pyrex substrates were grain boundaries (Figs 5a–d, 6a and b). Predendritic, cellular microstructure could be observed in splats quenched on the aluminium and copper substrates. The Pyrex substrates, however, had markedly larger grains than those exhibited in splats quenched on the other two substrates, which were not

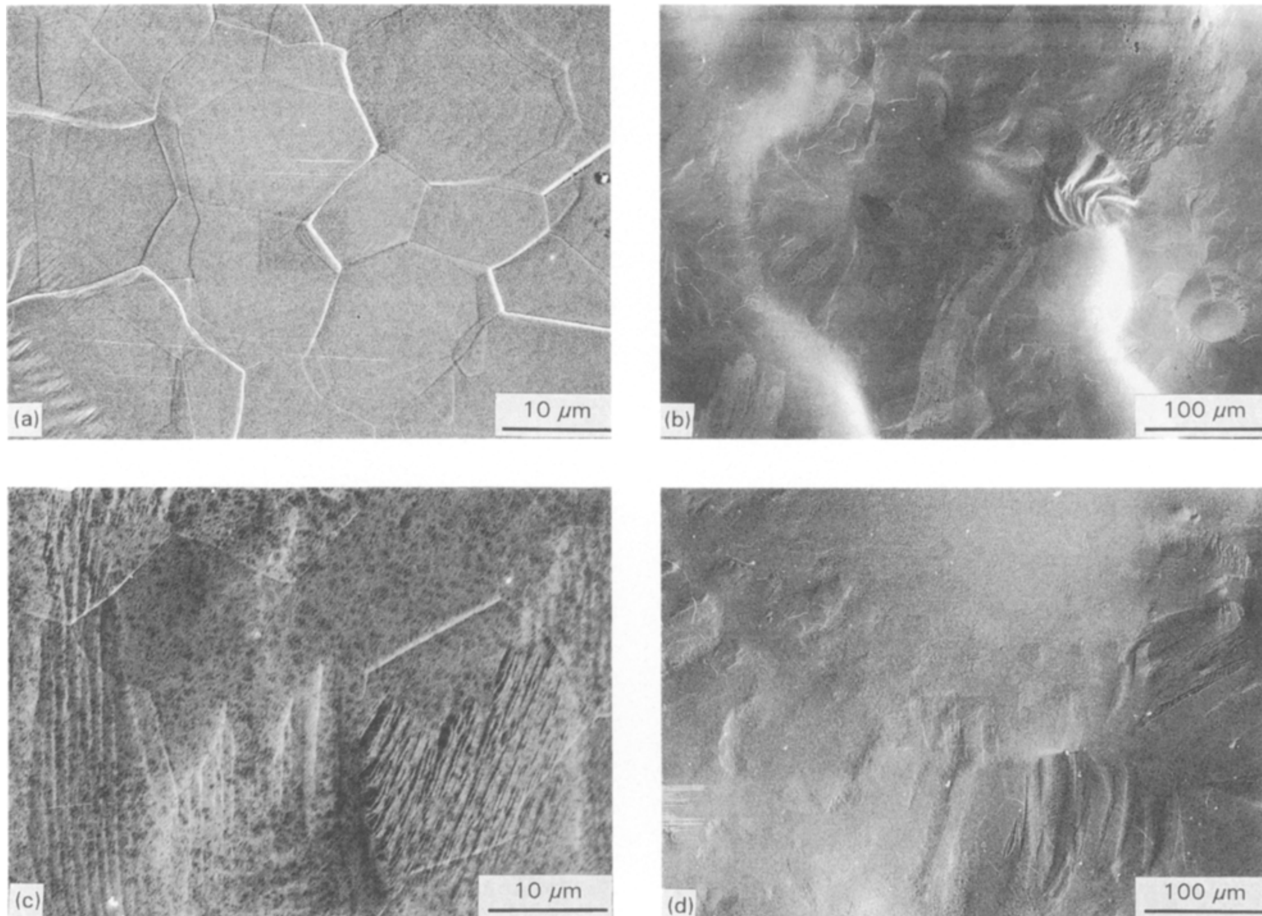

Figure 5 Photographs of top surfaces of splats quenched on (a, b) copper and (c, d) aluminium. Data represented by the following conditions for copper and aluminium, respectively: initial droplet temperature 495/502 °C, initial substrate temperature 25/25 °C, droplet diameter 3.0/3.0 mm, free-fall distance 30/30 cm, spread factor 4.0/4.0.

cellular. The smallest grains observed on splats quenched on Pyrex were of the order of 100 μm. In contrast, the average grain size of splats quenched on both copper and aluminium was about 10 μm. There was no easily discernible difference in grain sizes between splats quenched on aluminium and copper.

Grain boundaries could be identified on both surfaces of the splat, although with more difficulty on the bottom surface, and there was no apparent difference in grain size between the top and bottom surfaces. There also was no observed effect of substrate temperature or free-fall distance (impact velocity) on the microstructure grain size. It can be concluded that the grain size was largely influenced by the thermal conductivity of the substrate material, indicating that this may be the most influential parameter, in this experiment, with regard to the cooling rate imposed on the splat.

For the sake of a comparison, a few droplets were splat-quenched from 15 cm on to a Teflon substrate (Fig. 6c and d). Teflon has very poor conducting properties ($0.35 \mathrm{W m^{-1} K^{-1}}$) such that the process of "splat-quenching" could no longer be considered rapid. Inspection of the top surface of the splat revealed rigorous dendritic growth as compared with the rapidly solidified splats produced on the other substrate materials. No cellular, predentritic microstructures, characteristic of the more rapidly solidified splats, were observed.

The bottom surfaces of the solidified splats are also worth examining through electron microscopy (Fig. 7). It was apparent from inspection of the splat bottom surfaces that the Pyrex substrate must have been much smoother than either the aluminium or copper substrates. Indeed, this was the case; the Pyrex substrate surface was polished while the aluminium and copper substrate surfaces were only sanded smooth. While the bottom surface of the splats quenched on the Pyrex substrate were relatively smooth (Fig. 7c), the bottom surfaces of the splats quenched on the aluminium and copper substrates exhibited the imprints of the rough substrate surfaces (Fig. 7a and b).

One of the most important heat transfer considerations involved in the splat-quenching process is the quality of the thermal contact at the splat–substrate interface. In general, one might expect a rough substrate surface to improve thermal contact because of the increased potential contact area. However, this seemed not to be necessarily the case judging by the poor adhesion of the splats to either the copper or aluminium substrates. Adhesion between the splat and both the copper and aluminium substrates was so poor that stresses introduced in the splat during solidification caused it to curl a small amount on the substrate surface. In contrast, splats quenched on the Pyrex substrate tended to have better adhesion, requiring the use of a razor blade for their removal.

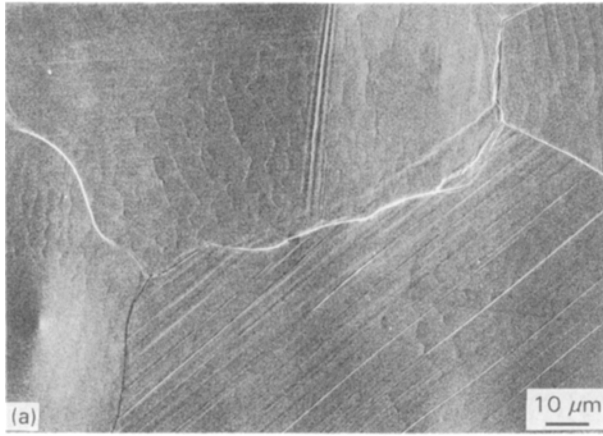

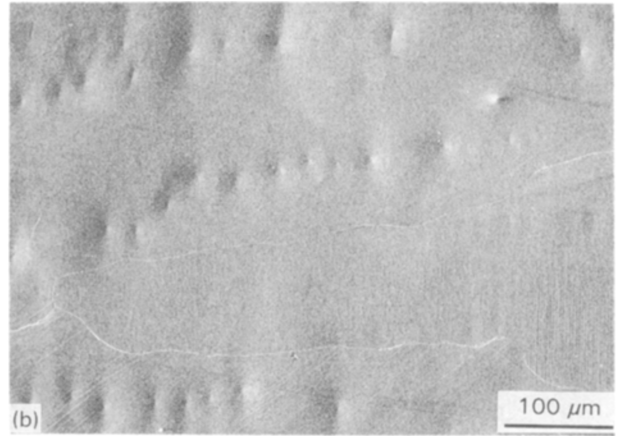

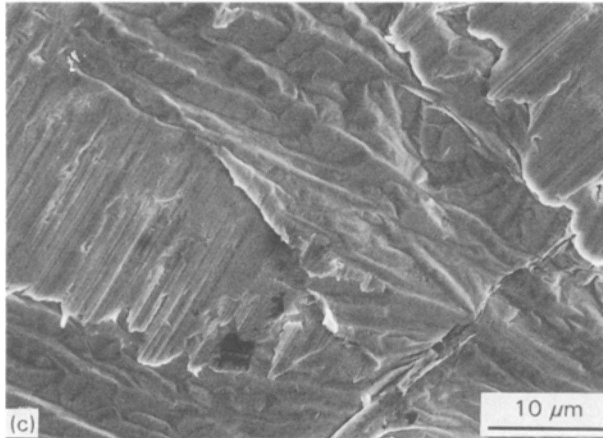

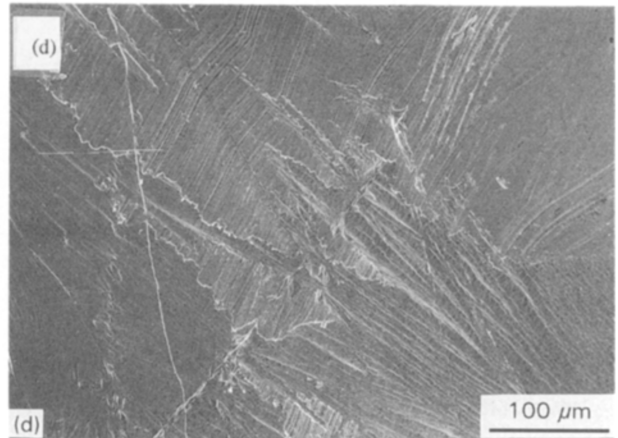

Figure 6 Photographs of top surfaces of splats quenched on (a, b) Pyrex and (c, d) Teflon. Data represented by the following conditions for Pyrex and Teflon, respectively: initial droplet temperature 492/497 °C, initial substrate temperature 25/25 °C, droplet diameter 3.0/3.0 mm, free-fall distance 30/30 cm, spread factor 4.2/4.3.

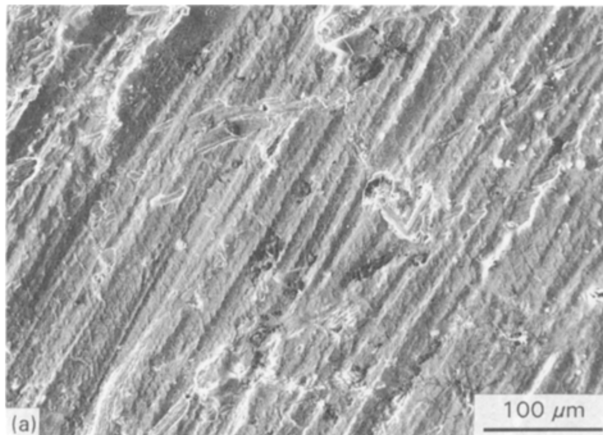

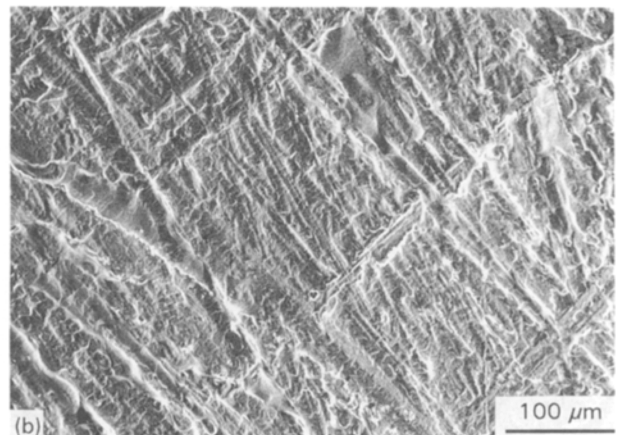

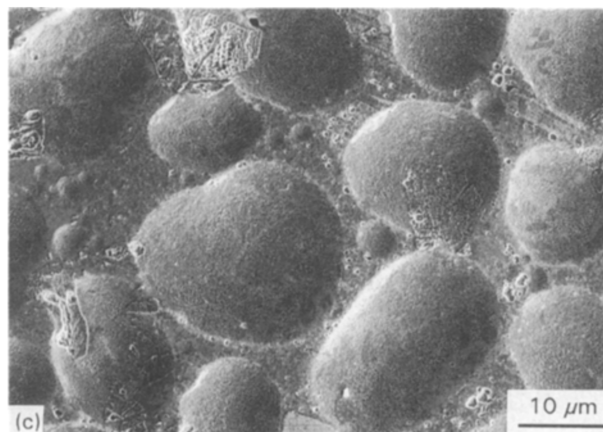

Figure 7 Photographs of bottom surfaces of splats quenched on (a) aluminium, (b) copper and (c) Pyrex. Data represented by following conditions for aluminium, copper and Pyrex, respectively: initial droplet temperature 502/495/495 °C, initial substrate temperature 25/25/25 °C, droplet diameter 3.0/3.0/2.9 mm, free-fall distance 30/30/30 cm, spread factor 4.0/4.0/4.2.

However, entrapped air makes itself apparent with the Pyrex substrate by leaving pox marks on the bottom surface of the solidified splat (Fig. 7c). The evolution of these air bubbles at the interface is an interesting subject. Initially, the volume of air entrapped within the interface might have been quite small. However, as

the interface is heated the entrapped air expands, reducing the degree of thermal contact between the splat and substrate.

A possible mechanism affecting the extent of undercooling of the melt is the nature of the spreading of the splat on the affecting surface. Although it is difficult to ascertain exactly how the flow influences early nucleation, it is conceivable that the relative stability of the flow could be influential. A simple means of manipulating the flow characteristics can be achieved through changing the impact velocity, by changing the free-fall distance of the droplet above the substrate. An appropriate indicator for the nature of the flow can be given by the impact Reynolds number, defined by the droplet diameter and impact velocity.

Figure 8 shows the approximate undercooling versus Reynolds number (defined in the nomenclature) over a range of Reynolds numbers from 2700 to 3900. These data were collected using an aluminium substrate at room temperature. The free-fall distance was varied from 15 to 30 cm above the substrate surface. Despite the large spread of the data, Fig. 8 indicates that indeed the amount of undercooling exhibited by the splat seems to be dependent on the nature of the flow. As the Reynolds number increases, solid nucleation appears to be more probable and the amount of undercooling decreases. The reasons for this result are not straightforward and they are dependent on the complex interaction between the liquid metal flow and the microscopic structure of the substrate surface. We feel that future experiments should be designed with the aim of further investigating verifying and explaining the trend shown in Fig. 8.

One of the goals of the present study is to test the validity of the proposed theoretical model in predicting the experimental findings. Figs 9 and 10 present comparisons of theoretical and experimental results

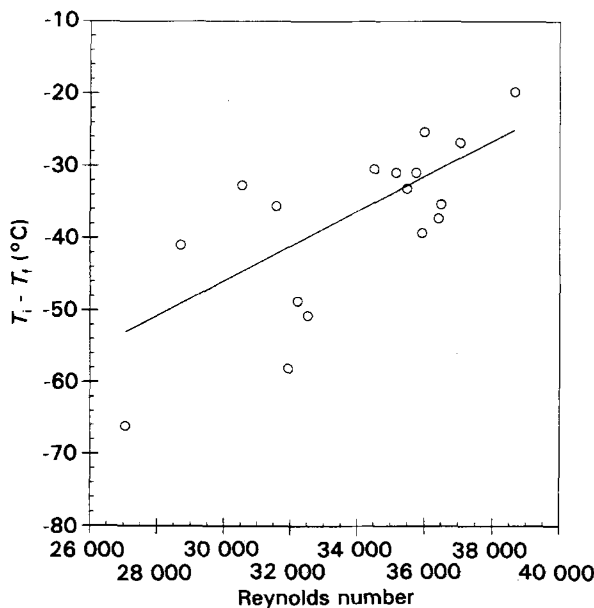

Figure 8 Effect of impact Reynolds number on undercooling of splat quenched on aluminium. Initial droplet temperature 485 ± 5 °C, initial substrate temperature 25 °C, droplet diameter 3.0 ± 0.3 mm, free-fall distance 15–30 cm.

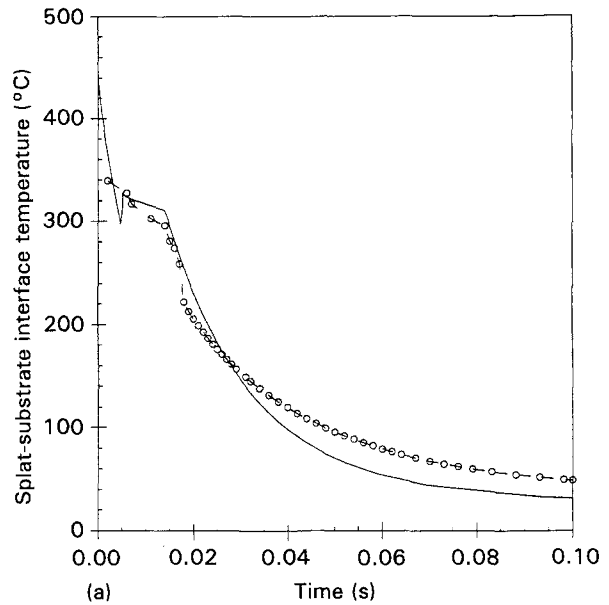

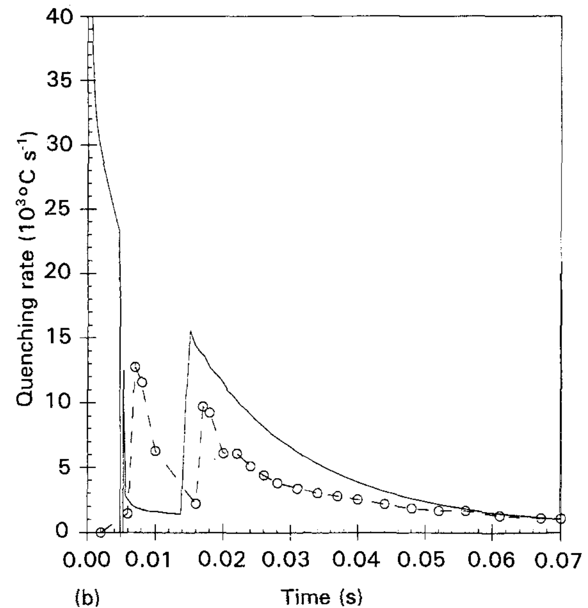

Figure 9 Comparison of (○) experimental and (——) numerical results for splat-quenching on the copper substrate: (a) splat–substrate interface temperature versus time, (b) splat-quenching rate versus time. Experimental results: initial droplet temperature 468 °C, initial substrate temperature 25 °C, droplet diameter 3.0 mm, free-fall distance 30 cm, spread factor 4.1. Numerical results: initial splat temperature 460 °C, initial substrate temperature 25 °C, droplet diameter 3.0 mm, spread factor 4.1, heat transfer coefficient 15 kW m^{-2} K^{-1}, undercooling 40 °C.

for the temperature and quenching rate histories at the splat–substrate interface. A copper substrate was used in Fig. 9 and a Pyrex substrate in Fig. 10. The initial temperature of both substrates was 25 °C. The numerical model for the results in Fig. 9 duplicated the experimental condition of a 3 mm lead droplet released from 30 cm above the substrate with a temperature at release time of 468 °C. The temperature at impact time was estimated to be (see Appendix) 460 °C. The experimentally measured spread factor was 4.1. The heat transfer coefficient at the splat–substrate interface that defines the contact resistance was assumed to be $h_c = 15 kW/m^2K$. This

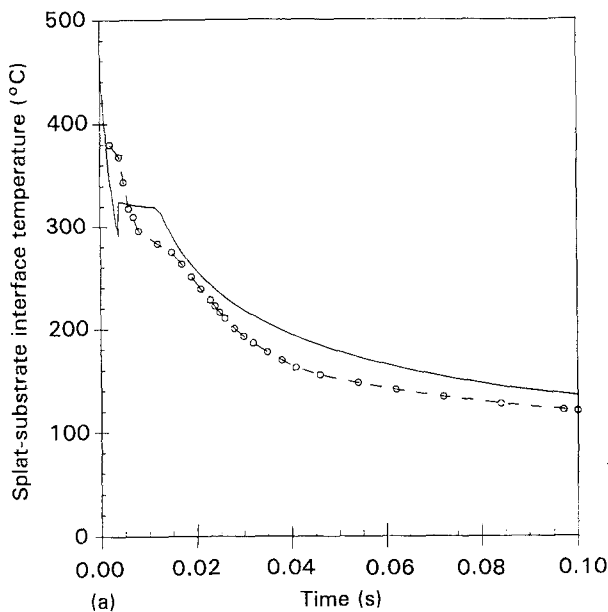

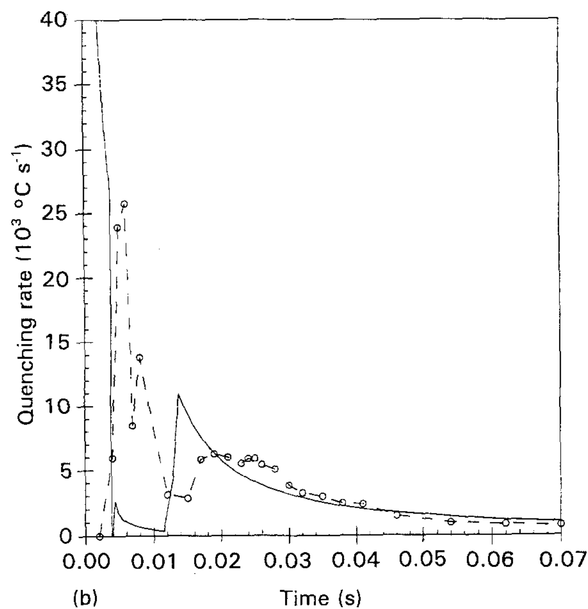

Figure 10 Comparison of (○) experimental and (——) numerical results for splat-quenching on the Pyrex substrate: (a) splat–substrate interface temperature versus time, (b) splat-quenching rate versus time. Experimental results: initial droplet temperature 494 °C, initial substrate temperature 25 °C, droplet diameter 2.7 mm, free-fall distance 30 cm, spread factor 4.4. Numerical results: initial splat temperature 486 °C, initial substrate temperature 25 °C, droplet diameter 2.7 mm, spread factor 4.4, heat transfer coefficient 100 kW m^{-2} K^{-1}, undercooling 40 °C.

value is within the ranges reported in the literature and was chosen so as to yield the best agreement between the theoretical model and the experiment. The effect of h_c on the results is discussed in a later part of this section.

The conditions for the results of Fig. 10 were similar. This time the lead droplet diameter was measured to be 2.7 mm, the droplet impact temperature 486 °C, the speed factor 4.4 and the contact heat transfer coefficient used was $h_c = 100kW/m^2K$.

Examining Figs 9 and 10, we conclude that the predictions of the model are satisfactory especially if one takes into account the relative simplicity of the model. The temperature of the splat–substrate interface decreases monotonically in both Figs 9a and 10a, except when solidification is initiated in the splat resulting, temporarily, in an increase in the temperature. The rate of cooling is very rapid initially, and slower after the completion of the freezing process.

Figures 9b and 10b present a more critical comparison between experimental and numerical results in the form of quenching rate versus time curves. It can be seen from these figures that after the quenching rates have become relatively small, the numerical and experimental results compare very favourably. At early times qualitative agreement is present, but the sluggish response of the thermocouples prohibits good

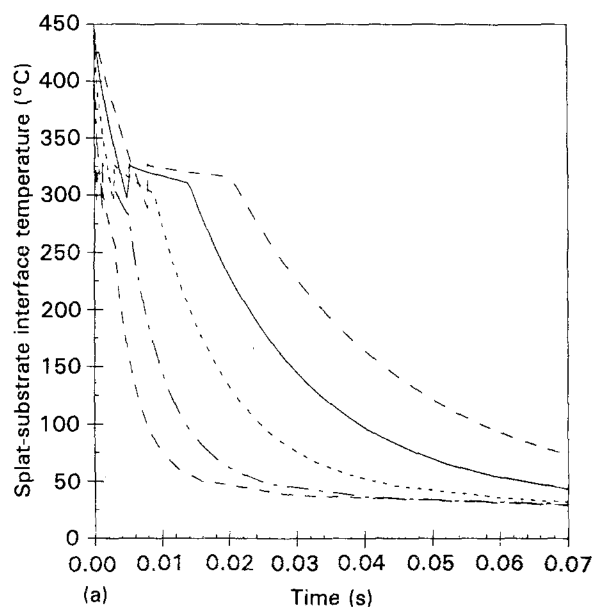

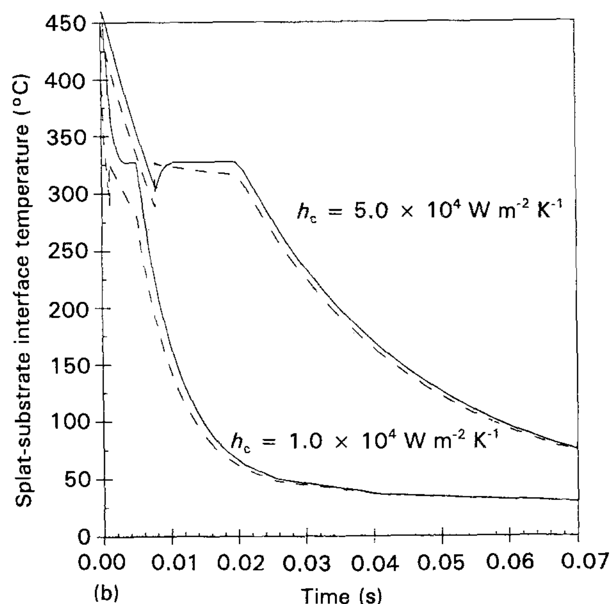

Figure 11 Effect of thermal contact resistance between splat and copper substrate on the thermal history of the splat: (a) thermal history of bottom-centre location of splat for a range of interface heat transfer coefficients, (b) thermal history of splat at (——) top and (– –) bottom surfaces. Initial splat temperature 460 °C, initial substrate temperature 25 °C, droplet diameter 3.0 mm, spread factor 4.1, undercooling 40 °C. For (a), h_c (W m^{-2} K^{-1}) = (– –) 1.0×10^4 (uppermost curve), (——) 1.5×10^4, (– – –) 2.5×10^4, (– – –) 5.0×10^4, (– –) 1.0×10^5 (lowermost curve).

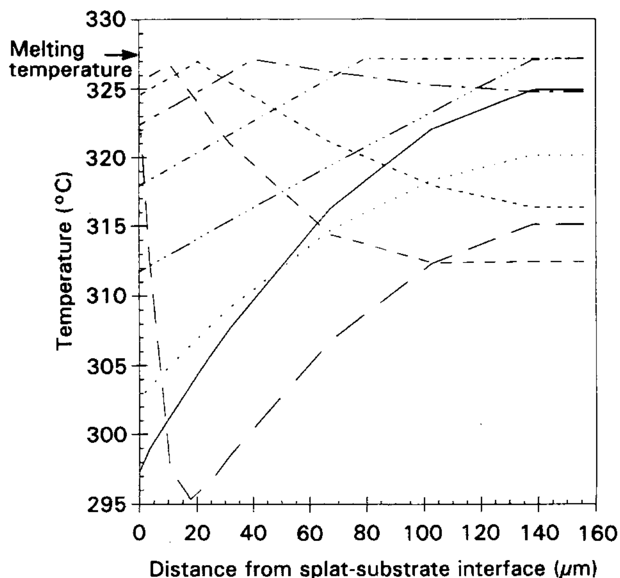

Figure 12 Axial temperature profiles across splat quenched on copper during freezing. Initial splat temperature 460 °C, initial substrate temperature 25 °C, droplet diameter 3.0 mm, spread factor 4.1, heat transfer coefficient 15 $\mathrm{kW\,m^{-2}\,K^{-1}}$, undercooling 40 °C. t (ms) = (——) 4.74, (– –) 5.13, (— — —) 5.31, (- - -) 5.65, (– – –) 6.60, (–·–) 9.08, (–····–) 13.08, (· · ·) 14.54.

quantitative agreement between theory and experiment.

The importance of the thermal contact resistance has made itself clear in the experimental portion of this study. The numerical model was used to further explore and establish quantitatively the effect of the contact thermal resistance. Figure 11 shows the numerical results on the thermal history of splats quenched with varying degrees of thermal contact quality. It can be seen that the effect is substantial. Figure 11a shows the thermal histories of the bottom-centre surface node of the splat for interface heat transfer coefficients (h_c) ranging from 10 to 100 $\mathrm{kW\,m^{-2}\,K^{-1}}$. It can be seen that as the interface heat transfer coefficient becomes small (poor thermal contact), its effect dominates the cooling rate of the splat (Newtonian cooling). Conversely, as the heat transfer coefficient becomes larger, its effect becomes less influential on the cooling rate of the splat (ideal cooling). It is also clear that the interface heat transfer coefficient has a significant influence over the length of time required to initiate freezing as well as over the duration of the freezing process.

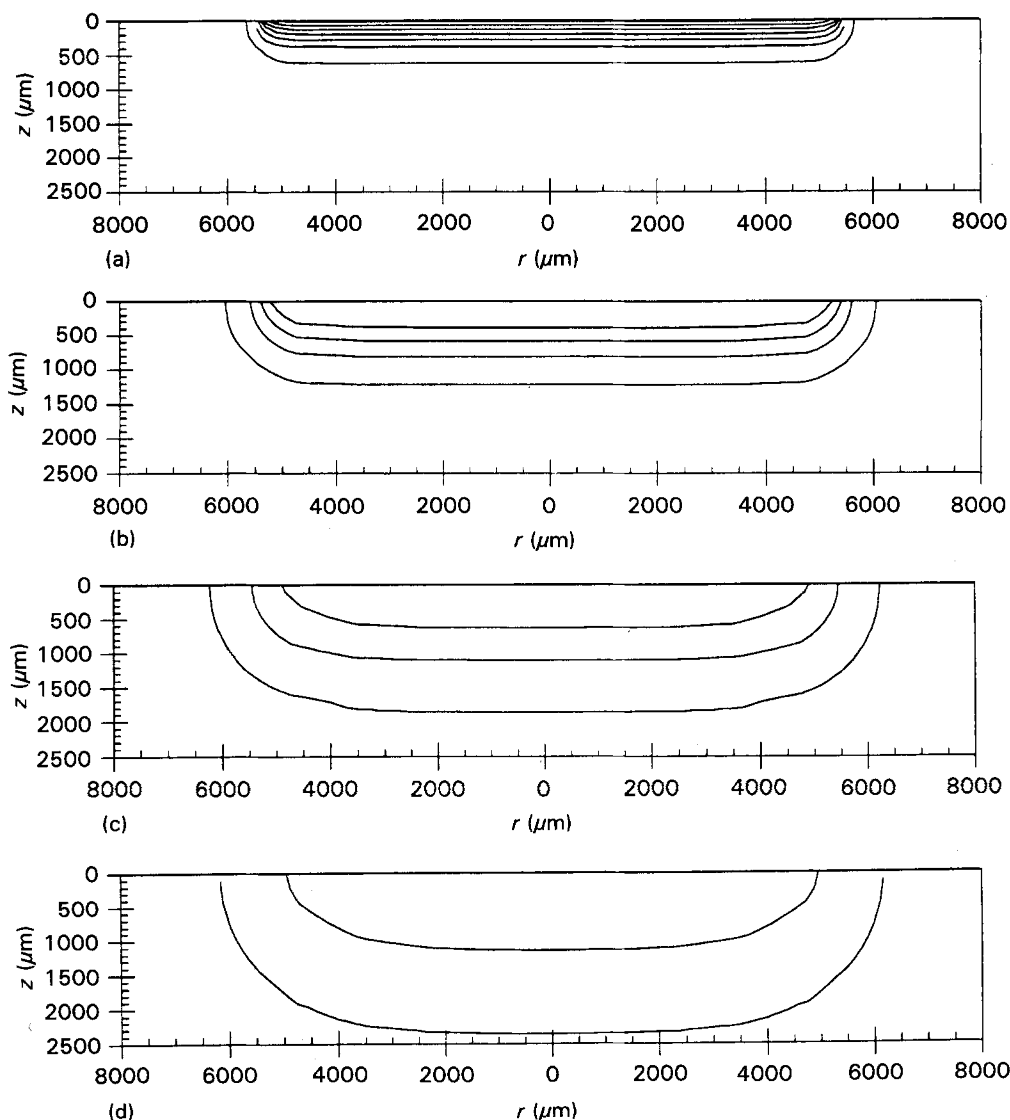

Figure 13 Transient isotherms in the copper substrate at t(s) = (a) 5.0×10^{-4}, (b) 2.0×10^{-3}, (c) 5.0×10^{-3}, (d) 1.0×10^{-2}. Initial splat temperature 460 °C, initial substrate temperature 25 °C, droplet diameter 3.0 mm, spread factor 4.1, heat transfer coefficient 100 $\mathrm{kW\,m^{-2}\,K^{-1}}$, undercooling 40 °C. 10 °C per isotherm; outermost isotherm = 30 °C.

Fig. 11b compares the thermal histories of centreline nodes at the top and bottom surfaces of the splat for two interface heat transfer coefficients. It can be seen that during the initial period of quenching, the temperature difference between the top and bottom surfaces can be substantial especially if the thermal contact between the splat and substrate is good (high h_c).

A characteristic feature of the numerical results of Figs 9 to 11 is the undercooling dip appearing just prior to the onset of freezing. This is an interesting detail which experimental results were unable to detect clearly. Referring back to Fig. 9a, it is apparent that the heat extraction is insufficient to sustain the undercooling achieved prior to solidification, i.e. the kinetics of crystalline formation is fast enough so that the rate of latent heat released is sufficient to substantially reheat the splat. This is an observation worth further consideration, because it indicates that despite the original undercooling, the interface freezing temperature may quickly rise to the melting temperature. Our interest in this consideration stems from the fact that microstructural features of the resulting solid are largely determined by the rate of solidification, which is dictated by thermal conditions at the freezing interface.

Details of the transient thermal conditions within the splat during its solidification obtained numerically are presented in Fig. 12. For the sake of clarity there are relatively few time steps presented. It can be seen that the freezing interface temperature rises to within 1 °C of the melting temperature after this interface has propagated only 10 μm into the splat ($t = 5.13$ ms). This result informs us that recalescence is confined to a relative small region adjacent to the contact surface. Hence, the enhanced solidification speed afforded by undercooling the melt is largely ineffectual in influencing the gross properties of the splat when thermal

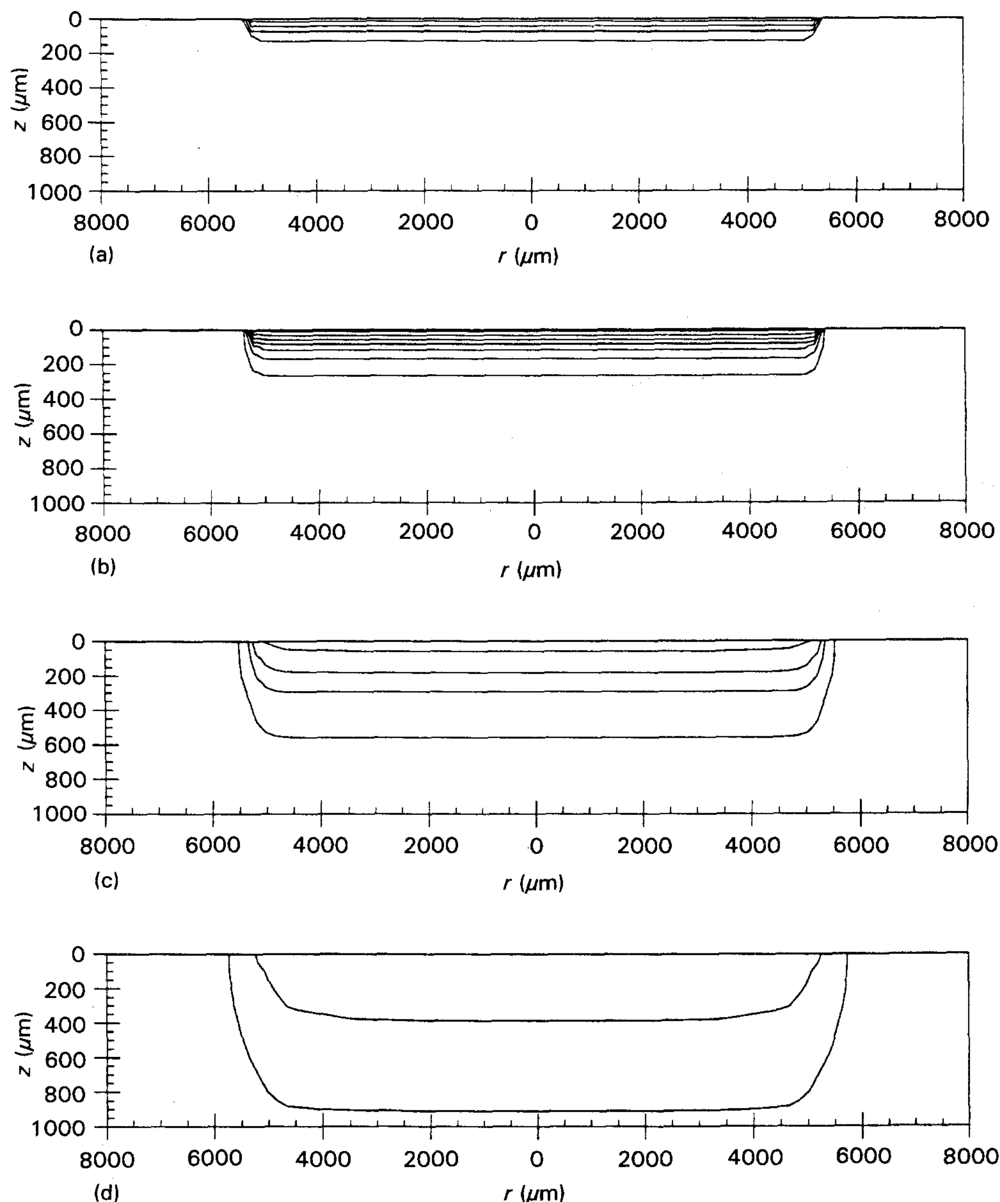

Figure 14 Transient isotherms in the Pyrex substrate at t(s) = (a) 1.0×10^{-3}, (b) 1.0×10^{-2}, (c) 5.0×10^{-2}, (d) 2.0×10^{-1}. Initial splat temperature 486 °C, initial substrate temperature 25 °C, droplet diameter 3.0 mm, heat transfer coefficient 100 kW m^{-2} K^{-1}, undercooling 40 °C. (a) 80 °C per isotherm, (b–d) 40 °C per isotherm; outermost isotherm = 40 °C.

contact with the substrate is poor ($h_c = 15$ kW $m^{-2} K^{-1}$ in Fig. 12) and the splat thickness is relatively large (156 μm in Fig. 12). The evaluation of thermal conditions within the splat, shown in Fig. 12, also demonstrates that linear temperature gradients are established below the freezing interface.

One of the distinctive attributes of the present numerical solution to the splat-quenching problem is that it accounts for two-dimensional conduction into the substrate. Previous investigations into this system have assumed that the conduction of heat into the substrate can be treated as one-dimensional. Figs 13 and 14 examine the actual transient temperature field within a copper and a Pyrex substrate, respectively.

Figure 13 shows the dissipation of heat into a copper substrate, assuming close to ideal thermal contact between the splat and substrate ($h_c = 100$ kW $m^{-2} K^{-1}$). The evolution and decay of thermal gradients in the substrate is very rapid. The substrate surface temperature reaches a peak of approximately 95 °C during the period in which latent heat is released while the splat freezes. The elevation of temperature much beyond the outside radius of the splat (5370 μm) is marginal, especially in the initial period of quenching. For most of the very early period in which heat is being removed from the splat, isotherms developing beneath the splat are flat, indicating one-dimensional conduction in the substrate material. The long-term transfer of heat away from the vicinity of splat, however, becomes significantly two-dimensional as demonstrated by the curvature of the isotherms.

Figure 14 shows the development of isotherms in the Pyrex substrate using a contact resistance of coefficient $h_c = 100$ kW $m^{-2} K^{-1}$. It is apparent that the low conductivity of Pyrex results in a much slower dissipation of heat into the substrate, even though the thermal contact between splat and substrate is very good. The low conductivity of the material also produces higher thermal gradients, greater heating of the splat–substrate interface, and less heat penetration than exhibited by the copper substrate (Fig. 13). Unlike the copper substrate (Fig. 13), the Pyrex surface temperature (beneath the splat) does not attain its maximum value during the release of the latent heat of freezing. Instead, the maximum surface temperature occurs close to the time of initial contact. The temperature field stays largely one-dimensional for a longer period of time than that of Fig. 13 for the copper substrate.

5. Conclusions

In this paper a combined theoretical and experimental study was presented for the problem of solidification of a liquid metal droplet impacting on a cold substrate. The theoretical model accounted for two-dimensional conduction in the system.

It was found that the thermal conductivity of the substrate has an important effect on the cooling of the splat. Increasing the initial substrate temperature had a minimal effect on the process of splat-cooling. A significant amount of undercooling existed in all experiments and was accounted for in the theoretical modelling. The undercooling seems to decrease with increasing impact velocity of the droplet.

The thermal contact between the splat and the substrate was better in the case of a Pyrex substrate. Even in this case, pockets of entrapped air caused indentations on the bottom surface of the splat. The numerical model was used to illustrate the significant effect of the contact resistance on the freezing process.

The substrate conductivity markedly affected the grain size of the solidified splats. The grain size in the splats increased tenfold between copper or aluminium and Pyrex substrates. Splats solidified on Teflon (low thermal conductivity) exhibited dendritic microstructure with no cellular grain structure.

Despite the relatively high quenching rates and significant undercooling of the splat, the majority of solidification was found to occur principally under heat-transfer-limited conditions, i.e. the propagation of the freeze was not dominantly controlled by crystallization kinetics. Recalescence, where propagation of the freeze is not heat-transfer-limited, was confined to the region adjacent to the substrate surface, and consisting of less than 10% of the splat thickness. This observation was particular to a relatively thick splat (160 μm) in good contact with the substrate.

The two-dimensional nature of conduction within the substrate was also investigated. It was evident from the temperature field that conduction of heat from the splat into the substrate starts out one-dimensional, but becomes increasingly two-dimensional as heat penetrates deeper into the substrate–more so for conductive substrates. Two-dimensional effects seem not to predominate very early in the quenching process. However, bulk heat removal from the immediate vicinity of the substrate beneath the splat is highly influenced by both radial and axial heat transfer, such that the determination of long-term thermal conditions must be accomplished with a two-dimensional model.

References

1. H. JONES, "Rapid Solidification of Metals and Alloys", Monograph 8 (Institution of Metallurgists, London, 1982).
2. E. GUTIERREZ-MIRAVETE, PhD thesis, Massachusetts Institute of Technology (1985).
3. S. ANNAVARAPU, D. APELIAN, and A. LAWLEY, *Metall. Trans.* **21A** (1990) 3237.
4. R. H. BRICKNELL, *ibid.* **7A** (1986) 583.
5. R. G. BROOKS, C. MOORE, A. G. LEATHAM and J. S. COOMBS, *Powder Metall.* **2** (1977) 100.
6. T. R. ANANTHARAMAN and C. SURYANARAYANA, *J. Mater. Sci.* **6** (1971) 1111.
7. P. PREDECKI, A. W. MULLENDORE and N. G. GRANT, *Trans. Metall. Soc. AIME* **233** (1965) 1581.
8. W. E. BROWER Jr, R. STRACHAN and M. C. FLEMINGS, *AFS Cast Met. Res. J.* **6** (1970) 176.
9. M. G. SCOTT, *J. Mater. Sci.* **9** (1974) 1372.
10. G.-X. WANG and E. F. MATTHYS, *Int. J. Rapid Solidifi.* **6** (1991) 141.
11. *Idem, Int. J. Heat Mass Transf.* **35** (1992) 141.
12. P. H. SHINGU and R. OZAKI, *Metall. Trans.* **6A** (1975) 33.
13. D. E. ROSNAR and M. EPSTEIN, *Chem. Eng. Sci.* **30** (1975) 511.

14. P. V. EVANS and A. L. GREER, *Mater. Sci. Eng.* **98** (1988) 357.
15. P. MATHUR, D. APELIAN and A. LAWLEY, *Acta Metall.* **37** (1989) 429.
16. E. GUTIERREZ-MIRAVETE, E. J. LAVERNIA, G. M. TRAPAGA, J. SZEKELY and N. J. GRANT, *Metall. Trans.* **20A** (1989) 71.
17. W. RANZ and W. MARSHALL, *Chem. Eng. Prog.* **48** (1952) 141.
18. D. A. ANDERSON, J. C. TANNEHILL and R. H. PLETCHER, "Computational Fluid Mechanics and Heat Transfer". (Hemisphere, New York 1984) p. 117.
19. T. D. BENNETT, MS thesis, University of Illinois at Chicago (1993).

Received 23 November 1992
and accepted 1 September 1993

Appendix: Convective cooling of the droplet during free fall

The initial droplet temperature at the time of release can be measured directly; however, there is no simple way of accurately measuring the impact temperature of the droplet. Therefore, in order to estimate the initial conditions of the splat on the substrate surface, the amount of cooling undergone by the droplet during free fall must be calculated.

Assuming lumped heat capacity and Newtonian cooling, the governing differential equation for the droplet temperature during free fall is given by

$$\frac{d}{dt}(\rho c\theta) = -h\theta \qquad (A1)$$

where θ is the instantaneous temperature difference between the droplet and the isothermal ambient air.

The convection coefficient can be found from Ranz and Marshall's [17] Nusselt number correlation for free-falling spheres:

$$Nu_D = \frac{hD}{k} = 2 + 0.6Re^{1/2}Pr^{1/3} \qquad (A2)$$

where, although the Prandtl number Pr can be considered a constant, the Reynolds number Re is a function of velocity, and hence a function of time:

$$Re = \frac{uD}{\nu} = \frac{gtD}{\nu} \qquad (A3)$$

Combining Equations A1 and A2 yields

$$\frac{d\theta}{dt} + \frac{\alpha Nu_D}{D}\theta = 0 \qquad (A4)$$

Equation A4 is a first-order linear differential equation which has the initial condition

$$\theta(t = 0) = \theta_a \qquad (A5)$$

where θ_a is the initial temperature difference between the droplet and ambient air.

The solution of Equation A4 subject to the initial Condition A5 reads

$$\theta = \theta_a \exp\left[-(2 + 0.4Re^{1/2}Pr^{1/3})\frac{\alpha t}{D}\right] \qquad (A6)$$

Equation A6 can be used to estimate the droplet temperature at any time during its flight. If the distance between the release point of the droplet and the substrate is denoted by L, the time elapsed between release and initial contact with the substrate is

$$t_c = \left(\frac{2L}{g}\right)^{1/2} \qquad (A7)$$

The temperature at impact is then estimated by evaluating Equation A6 at $t = t_c$ from Equation A7 after taking into account the time dependence of Re (Equation A3).

The impact velocity of the droplet is estimated via the free-fall equation in the gravitational field:

$$u = gt_c = (2gL)^{1/2} \qquad (A8)$$